Boundary-Layer Meteorology (2005) 114: 439–460

PARAMETERIZING TURBULENT EXCHANGE OVER SEA ICE: THE ICE STATION WEDDELL RESULTS

EDGAR L ANDREAS[1,*], RACHEL E. JORDAN[1]
and ALEKSANDR P. MAKSHTAS[2,3]

[1] *U.S. Army Cold Regions Research and Engineering Laboratory, 72 Lyme Road, Hanover, New Hampshire 03755-1290, U.S.A.;* [2] *International Arctic Research Center, 930 Koyukuk Drive, Fairbanks, Alaska 99775-7335, U.S.A.;* [3] *Arctic and Antarctic Research Institute, 38 Bering Street, St. Petersburg, 199397, Russia*

(Received in final form 23 February 2004)

Abstract. A 4-month deployment on Ice Station Weddell (ISW) in the western Weddell Sea yielded over 2000 h of nearly continuous surface-level meteorological data, including eddy-covariance measurements of the turbulent surface fluxes of momentum, and sensible and latent heat. Those data lead to a new parameterization for the roughness length for wind speed, z_0, for snow-covered sea ice that combines three regimes: an aerodynamically smooth regime, a high-wind saltation regime, and an intermediate regime between these two extremes where the macroscale or 'permanent' roughness of the snow and ice determines z_0. Roughness lengths for temperature, z_T, computed from this data set corroborate the theoretical model that Andreas published in 1987. Roughness lengths for humidity, z_Q, do not support this model as conclusively but are all, on average, within an order of magnitude of its predictions. Only rarely are z_T and z_Q equal to z_0. These parameterizations have implications for models that treat the atmosphere-ice-ocean system.

Keywords: Air–sea–ice interaction, Eddy-covariance measurements, Ice Station Weddell, Roughness lengths, Sea Ice, Turbulent surface fluxes.

1. Introduction

Ice Station Weddell (ISW) was an ideal site for micrometeorological research. Between February and early June 1992, ISW drifted northward in the western Weddell Sea, paralleling the track of the legendary *Endurance* (Gordon and Lukin, 1992; ISW Group, 1993). As such, ISW was always at least 300 km from any land, and our surface-level micrometeorological measurements were, therefore, over a very homogeneous, planar sea ice site with no topographic complications. Because our measurements were in the austral fall and early winter at latitudes between 66° and 72° south, the diurnal signal in the atmospheric forcing variables was weak. As a result, the atmospheric boundary layer was often in a quasi-steady state. We thus had a great

* E-mail: eandreas@crrel.usace.army.mil

opportunity to study the stable boundary layer, which is typically more ephemeral at lower latitudes (cf. Andreas et al., 2000).

Andreas and Claffey (1995) show the drift track of Ice Station Weddell and the duration of our measurement program. The micrometeorological observations on ISW included eddy-covariance measurements of the momentum, sensible and latent heat fluxes that ran almost continuously from 25 February (Julian day 56) through 29 May 1992 (day 150). From these, we develop and test parameterizations for the roughness lengths for wind speed, temperature, and humidity – z_0, z_T, and z_Q, respectively. In particular, our z_Q values constitute the largest set of values yet published that have resulted from eddy-covariance measurements over a snow-covered surface.

The z_0 values exhibit three aerodynamic regimes: an aerodynamically smooth regime, where viscosity is important in setting z_0; a saltation regime, where z_0 scales with the height of the saltation layer; and an intermediate region between these two extremes, where the fundamental roughness of the surface sets z_0. The ratios z_T/z_0 and z_Q/z_0 tend to corroborate Andreas's (1987) theoretical model. That is, both ratios decrease with increasing roughness Reynolds number. Thus, rarely do z_T and z_Q equal z_0, which is a common assumption in many models.

2. Turbulence Measurements

Ice Station Weddell was a multidisciplinary, joint Russian–American expedition. Research during the 4-month drift of the station included oceanography, biology, sea ice physics, and meteorology. Andreas and Claffey (1995), Andreas (1995), Makshtas et al. (1998, 1999), and Andreas et al. (2000) have already reported some of our meteorological research on ISW.

The meteorological site on ISW featured a hut with an electronics lab and sleeping quarters. Near this hut, we had several masts and towers that held our near-surface meteorological instruments. Andreas et al. (2004) describe the full suite of near-surface measurements we made on ISW. For the turbulence analysis that is our emphasis here, we review only our eddy-covariance measurements of the turbulent fluxes and our supporting measurements of mean conditions, the wind speed profile, and the surface temperature.

2.1. Eddy-covariance measurements

The cornerstone of the main meteorological site was our 5-m tower. This was festooned with instruments for measuring mean and turbulence quantities 4.65 m above the snow surface. This tower rotated a full 360° so we could periodically align its sensors with the mean wind for optimal exposure.

On this main tower, we measured air temperature and dew-point (actually frost-point) temperature with a General Eastern 1200MPS. This device measures air temperature with a platinum resistance thermometer and dew-point temperature with a cooled mirror. A second platinum resistance thermometer just under the mirror senses the mirror's temperature, which is the dew-point temperature. Both sensors are in a white, aspirated radiation shield. We measured wind speed and direction at the same height on this tower with an R.M. Young propeller/vane (model 35003). This vane also let us align the tower instruments visually with the mean wind.

For measuring the turbulent fluctuations in temperature (t) and in the longitudinal (u), transverse (v), and vertical (w) components of the wind vector, we used a three-axis K-type sonic anemometer/thermometer made by Applied Technologies Inc. (ATI). We based the height at which we deployed this instrument, 4.65 m, on Kaimal and Finnigan's (1994, p. 219) suggestion. Because of its 0.15-m averaging paths, which degrade the instrument's ability to see eddies smaller than $2\pi \times 0.15$ m, they recommend that this sonic not be used below 4 m.

One key feature of this instrument is that the three sound paths are all orthogonal; therefore, mathematically rotating the measured wind vector into a frame that is horizontal and aligned with the mean wind involves simple trigonometry. Another key feature is that the three sound paths are separated. As a result, the measurements are less prone to flow distortion (e.g., Foken and Wichura, 1996). Finally, the remaining flow distortion has been studied and quantified (Kaimal et al., 1990); the system has firmware that corrects the output for this flow distortion in real time.

The temperature $\widetilde{T}_{\mathrm{son}}$ that sonic anemometers measure is a hybrid; specifically, it is (e.g., Schotanus et al., 1983; Kaimal and Gaynor, 1991; Larsen et al., 1993)

$$\widetilde{T}_{\mathrm{son}} = \widetilde{T}(1 + 0.51\widetilde{Q}), \tag{1}$$

where $\widetilde{T}$ is the true air temperature and $\widetilde{Q}$ is the specific humidity. The tildes denote instantaneous values. That is, the 'sonic temperature' is close to the virtual temperature (Bohren and Albrecht, 1998, p. 280),

$$\widetilde{T}_{\mathrm{v}} = \widetilde{T}(1 + 0.61\widetilde{Q}). \tag{2}$$

Thus, the sonic anemometer/thermometer is an ideal instrument for directly measuring the Obukhov length,

$$L = -\frac{\overline{T}_{\mathrm{v}}}{gk}\frac{u_*^3}{\overline{wt}_{\mathrm{v}}}. \tag{3}$$

Here u_* is the friction velocity, $(-\overline{uw})^{1/2}$, where $\overline{uw}$ is the kinematic momentum flux; $\overline{T}_{\mathrm{v}}$ is the average virtual temperature; g is the acceleration of

gravity; $k(=0.40)$ is the von Kármán constant; and $\overline{wt}_v$ is the turbulent vertical flux of virtual temperature.

When we are also interested in measuring the sensible heat flux $H_s \equiv \rho_a c_p \overline{wt}$, where ρ_a is the air density, c_p is the specific heat of air at constant pressure, and t is the turbulent fluctuation in actual air temperature, we need to consider carefully how to use the sonic temperature. Andreas et al. (1998), among others, show that

$$\overline{wt}_{son} = \overline{wt}(1 + 0.51\overline{Q}) + 0.51\overline{T}\,\overline{wq}. \tag{4}$$

Here $\overline{wt}$ is the kinematic sensible heat flux, $\overline{wq}$ is the kinematic latent heat flux, $\overline{T}$ and $\overline{Q}$ are the average air temperature and specific humidity, and $\overline{wt}_{son}$ is the flux we would compute if we correlated the measured sonic temperature fluctuations with the vertical velocity fluctuations.

When we define the Bowen ratio

$$Bo \equiv \frac{\rho_a c_p \overline{wt}}{\rho_a L_v \overline{wq}} = \frac{\overline{wt}}{D\overline{wq}}, \tag{5}$$

where L_v is the latent heat of evaporation or sublimation, we can rewrite (4) as

$$\overline{wt}_{son} = \overline{wt}\left[1 + 0.51\overline{Q} + \frac{0.51\overline{T}}{D\,Bo}\right]. \tag{6}$$

For Ice Station Weddell, $\overline{Q}$ was always less than $3.8 \times 10^{-3}\,\mathrm{kg\,kg^{-1}}$, $\overline{T}$ was less than 273 K, $D \equiv L_v/c_p$ was roughly 2500 K, and Bo was both positive and negative and had a magnitude that was typically at least 1 (Andreas and Cash, 1996). Consequently, for our measurements, $\overline{wt}_{son}$ is always within at least 5% of the true sensible heat flux $\overline{wt}$ and is only weakly biased because Bo was negative about 40% of the time. Because random errors in $\overline{wt}$ are always at least 10%, we henceforth use $\overline{wt}_{son}$ as the kinematic sensible heat flux with negligible error.

For measuring the turbulent fluctuations in water vapour density ρ_v, we used a Lyman-α hygrometer made by Atmospheric Instrumentation Research (AIR, now part of Vaisala). This was also mounted on our main tower, displaced horizontally about 0.25 m from the w path of the sonic anemometer. This Lyman-α is based on Buck's (1976, 1977) design. We used the analysis procedure that he reports (also given in the AIR manual) to deduce ρ_v from its measurements. Since Lyman-α hygrometers are known to drift, during our post-experiment processing, we calibrated its output for every hour using the recorded air temperature and dew-point temperature from the General Eastern 1200MPS nearby on the main tower.

2.2. Turbulence processing

Both our sonic anemometer/thermometer and the Lyman-α hygrometer provided analog outputs. We digitized these and all other signals at 10 Hz and stored these series on 65-megabyte cassette tapes using a data acquisition system made by Optim. Before being recorded, each signal passed through a noise and anti-aliasing filter with a –3 dB point at 5 Hz. During our post-processing, we computed hourly averages of all quantities measured on the tower. These hourly averages are what we use in our subsequent discussions.

The five turbulence variables, u, v, w, t, and ρ_v, of course, required extra handling. We first applied routine quality controls such as screening for and removing spikes and dropouts.

Before computing turbulence statistics, we also evaluated the linear trend in each hour series using the inverted Haar wavelet in the method that Andreas and Treviño (1996, 1997) developed. In this method, the decision on whether to remove a trend relies on comparing the slope of the computed linear trend μ_1 with the fundamental accuracy A of the instrument that produced the time series. For our processing, we removed the linear trend in any hourly series for which (see Andreas and Treviño, 1996, 1997)

$$\left|\frac{\mu_1^2\Delta^2 N(N+1)}{12}\right| > A^2. \tag{7}$$

Here $\Delta(=0.1\,\mathrm{s})$ is our sampling interval, and $N(=36,000)$ is the number of points in each series. Basically, (2.7) says we detrend only when the variance of the actual signal is greater by A^2 than the variance of the detrended signal. In other words, we cannot detect a trend that is below our measurement accuracy.

For the u, v, w, and t series, we used $0.02\,\mathrm{m\,s^{-1}}$, $0.02\,\mathrm{m\,s^{-1}}$, $0.02\,\mathrm{m\,s^{-1}}$, and 0.01 °C, respectively, for A in (7). Since the accuracy with which we can measure ρ_v with the Lyman-α hygrometer depends on the average water vapour density, $\overline{\rho}_v$, we set $A = 0.01\overline{\rho}_v$ in (7) for the Lyman-α data.

Although we could manually rotate the tower holding our turbulence instruments to point them into the wind, mathematically rotating the sonic wind components into the wind frame was still necessary during post-processing. Because the sonic measures three wind components, three rotations are necessary (e.g., McMillen, 1988; Baldocchi et al., 1988; Finnigan et al., 2003). To evaluate the three rotation angles, we imposed three constraints on the true wind vector: the hourly averaged wind vector had no vertical or transverse components (i.e., $\overline{W} = 0$ and $\overline{V} = 0$), and there was no crosswind component of the vertical momentum flux (i.e., $\overline{vw} = 0$).

Fluxes of concentration variables – in our case, water vapour – formally require a correction for the 'dilution effect' (Fairall et al., 2000) – the so-called Webb correction. Webb et al. (1980) and, more recently, Fairall et al.

(2000) and Fuehrer and Friehe (2002) discuss this correction and give approximate correction equations. From these references, we can show that the corrected latent heat flux (H_{Lc}) is related to the measured latent heat flux (H_{Lm}; after all detrending, rotations, etc.) by

$$H_{\mathrm{Lc}} = H_{\mathrm{Lm}}\left(1 + \frac{M_{\mathrm{a}}\overline{\rho}_{\mathrm{v}}}{M_{\mathrm{w}}\rho_{\mathrm{a}}}\right)\left(1 + \frac{\overline{\rho}_{\mathrm{v}}L_{\mathrm{v}}}{\rho_{\mathrm{a}}c_p\overline{T}}Bo\right). \tag{8}$$

Here, M_{a} is the molecular weight of air, and M_{w} is the molecular weight of water.

Because we made our measurements in temperatures generally well below 0 °C, the left bracketed term in (8) is essentially 1 for our dataset. In the second bracketed term in (8), the Bowen ratio (based on H_{Lm}) for our data was both positive and negative. The average of that second term is thus about 0.98, and individual values were more than 1–2% away from 1 only when H_{Lm} was measured to be very near zero. Hence, we did not make the Webb correction for any of our latent heat flux values because it was much smaller than the original uncertainty in these values.

Finally, after we detrended, averaged, and rotated coordinates, we screened the data manually to exclude questionable values. For example, the coordinate rotation was not always successful and, thus, produced turbulence quantities that seemed unrealistic. Therefore, we required of the coordinate rotation that the angle computed to produce $\overline{W} = 0$ was small. That is, we assumed that we had done of good job of leveling the sonic in the first place (cf. Finnigan et al., 2003). Second, we required that the angle computed to produce $\overline{V} = 0$ was roughly the same angle that the propeller/vane measured. If the rotated data failed these tests, we either excluded that hour's data from our analysis or used the unrotated data if they looked reasonable.

2.3. Wind speed profile

Andreas and Claffey (1995) report our measurements of near-surface wind speed profiles on ISW and calculate the drag coefficients implied by these measurements. Briefly, we had a thin mast with simple R.M. Young propeller anemometers (model 27103) mounted 0.5, 1, and 2 m above the snow surface. At 4 m on this mast, we had another R.M. Young propeller/vane (model 35003). We could rotate this mast and thus point the anemometers into the wind through an undisturbed upwind sector that was about 160° wide. We used the wind direction from the propeller/vane and assumed a cosine response to correct the lower three anemometers for misalignment with the mean wind. For evaluating z_0 from these profiles, we excluded any profiles for which the misalignment of the three simple propellers with the mean wind

was greater than 20°. Andreas and Claffey explain the other constraints that we imposed on these wind speed profiles to ensure that they were our best near-neutral cases.

2.4. Surface temperature

Because the snow surface temperature T_s is the key variable if we hope to evaluate the bulk transfer coefficients for sensible and latent heat, we measured it several ways. Andreas et al. (2004) describe our variety of surface temperature measurements in detail. Our primary measurement of the surface temperature, and the one we rely on in evaluating the scalar roughness lengths, was with a Barnes PRT-5 precision radiation thermometer. The blackbody temperature that the PRT-5 measures, T_{BB}, is related to the components of the net longwave radiation balance of the snow surface according to

$$\sigma T_{BB}^4 = \varepsilon\sigma T_s^4 + (1-\varepsilon)Q_{L\downarrow}. \tag{9}$$

Here $\sigma(=5.67051\times10^{-8}\,\mathrm{W\,m^{-2}\,K^{-4}})$ is the Stefan–Boltzmann constant, $Q_{L\downarrow}$ is our ISW measurement of incoming longwave radiation (Andreas et al., in press), and T_{BB} and T_s must both be in kelvins. For the surface emissivity ε, we use 0.99 (Warren, 1982; Dozier and Warren, 1982). That is, by rearranging (2.9), we could compute T_s from the measured PRT-5 blackbody temperature and the incoming longwave radiation. We estimate the accuracy of these T_s values to be $\pm0.5\,^{\circ}\mathrm{C}$.

3. Roughness Lengths

Numerical models of surface-atmosphere interaction need to predict the turbulent surface fluxes of momentum ($\tau \equiv \rho_a\overline{uw}$) and sensible ($H_s \equiv \rho_a c_p\overline{wt}$) and latent ($H_L \equiv L_v\overline{\rho_v w}$) heat. These predictions are generally through a bulk flux algorithm such that

$$\tau = \rho_a u_*^2 = \rho_a C_{Dr} U_r^2, \tag{10a}$$

$$H_s = \rho_a c_p C_{Hr}\, U_r(T_s - \Theta_r), \tag{10b}$$

$$H_L = \rho_a L_v C_{Er} U_r(Q_s - Q_r). \tag{10c}$$

Here, U_r, Θ_r, and Q_r are average values of the wind speed, potential temperature, and specific humidity at reference height r; T_s and Q_s are average surface temperature and specific humidity, this latter evaluated as the saturation value at T_s; and (10a) defines the friction velocity u_* that we use in the Obukhov length (3).

The key to the bulk flux algorithm is evaluating the drag coefficient (C_{Dr}) and the transfer coefficients for sensible (C_{Hr}) and latent (C_{Er}) heat appropriate for height r. These are related to the roughness lengths z_0, z_{T}, and z_{Q} according to (e.g., Garratt, 1992, p. 54f.)

$$C_{\mathrm{Dr}} = \frac{k^2}{[\ln(r/z_0) - \psi_{\mathrm{m}}(r/L)]^2}, \tag{11a}$$

$$C_{\mathrm{Hr}} = \frac{k^2}{[\ln(r/z_0) - \psi_{\mathrm{m}}(r/L)][\ln(r/z_{\mathrm{T}}) - \psi_{\mathrm{h}}(r/L)]}, \tag{11b}$$

$$C_{\mathrm{Er}} = \frac{k^2}{[\ln(r/z_0) - \psi_{\mathrm{m}}(r/L)][\ln(r/z_{\mathrm{Q}}) - \psi_{\mathrm{h}}(r/L)]}. \tag{11c}$$

Here, ψ_{m} and ψ_{h} are known corrections to the wind speed and scalar profiles that account for stratification effects. We use the same functions that Jordan et al. (1999) use. That is, for unstable stratification (i.e., $L < 0$), we use Paulson's (1970) functions. For stable stratification (i.e., $L > 0$), we use the formulation of Holtslag and De Bruin (1988) because these functions have the best properties in very stable stratification (Launiainen and Vihma, 1990; Jordan et al., 1999; Andreas, 2002). We make the usual assumption that ψ_{h} is the same for both the temperature and humidity profiles.

Sometimes, equations like (11) require that a displacement height d be subtracted from the r values to indicate the effective origin for the logarithmic profiles (e.g., Garratt, 1992, p. 86f.). Andreas (1995), however, develops a physically based model for flow over typical sea ice roughness elements and, with this, computes displacements heights to be usually less than 30 mm. In our earlier ISW profile analysis, Andreas and Claffey (1995) therefore ignored the displacement height, as we will here also.

Once z_0, z_{T}, and z_{Q} are known, computing the turbulent fluxes using (10) and (11) is straightforward. For example, we report tests of our ISW parameterizations in Andreas et al. (in press), where we simulate ISW exchange processes using SNTHERM, a one-dimensional mass and energy budget model. Although models like SNTHERM have parameterizations for these roughness lengths (Jordan et al., 1999), some are based on scanty data. In fact, for his recent review, Andreas (2002) found only a few reliable measurements of z_{Q} over surfaces of snow or ice.

With our ISW measurements of τ, H_{s}, and H_{L}, however, we can invert Equations (10) and (11) and thereby evaluate z_0, z_{T}, and z_{Q} in hopes of validating or improving parameterizations of these. The relevant equations are

$$z_0 = r \exp\left\{-\left[kC_{\mathrm{Dr}}^{-1/2} + \psi_{\mathrm{m}}(r/L)\right]\right\}, \tag{12a}$$

$$z_T = r \exp\left\{-\left[kC_{Dr}^{1/2}C_{Hr}^{-1} + \psi_h(r/L)\right]\right\}, \tag{12b}$$

$$z_Q = r \exp\left\{-\left[kC_{Dr}^{1/2}C_{Er}^{-1} + \psi_h(r/L)\right]\right\}. \tag{12c}$$

From out data, we calculate C_{Dr}, C_{Hr}, C_{Er}, and L from (10) and (3); z_0, z_T, and z_Q then result in turn. The reference height r is 4.65 m.

3.1. Momentum roughness

Figure 1 shows 740 estimates of z_0 as a function of u_*. Remember, these are based on hourly averages and eddy-covariance measurements of u_*.

We limit the z_0 values in Figure 1 to hours for which $u_* \geq 0.05\,\mathrm{m\,s^{-1}}$ and $U_r > 1\,\mathrm{m\,s^{-1}}$ since we have less confidence in both the z_0 and u_* values measured in light winds. We also eliminated hours for which z_0 was computed to be 0.1 m or more. Such values are erroneously large. These quality control tests eliminated only 74 h of data from the 812 h that yielded z_0 values. The $u_* \geq 0.05\,\mathrm{m\,s^{-1}}$ constraint eliminated most of these, 60 h.

These quality controls also eliminated cases from our analysis for which the stratification was very stable or very unstable. The maximum value of r/L (i.e., 4.65/L) for any of the z_0 values in Figure 1 or for the z_T and z_Q values in subsequent plots was 2.05; the minimum value was -1.56. From (12a), we deduce that this maximum value of r/L produced a maximum stratification correction that was roughly equal to the magnitude of $k\,C_{Dr}^{-1/2}$. In (12b) and (12c), the maximum correction for stable stratification had only about half

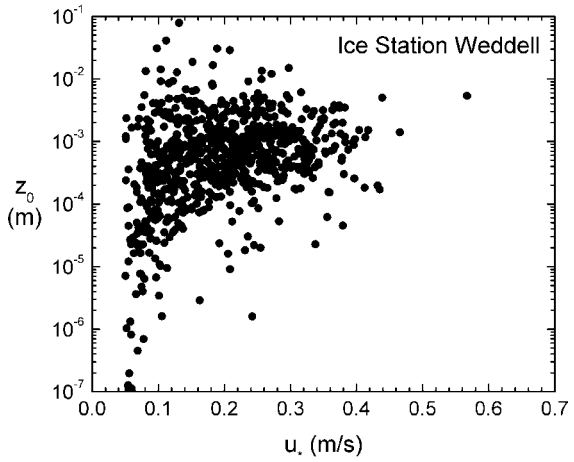

Figure 1. Hourly estimates of z_0 on Ice Station Weddell deduced from direct turbulence measurements of u_* and L and computations based on (12a).

the typical magnitudes of $kC_{\mathrm{Dr}}^{1/2}C_{\mathrm{Hr}}^{-1}$ and $kC_{\mathrm{Dr}}^{1/2}C_{\mathrm{Er}}^{-1}$. In unstable stratification, the maximum ψ_{m} and ψ_{h} values in (3.3) were only 15–20% of the corresponding $kC_{\mathrm{Dr}}^{-1/2}$, $kC_{\mathrm{Dr}}^{1/2}C_{\mathrm{Hr}}^{-1}$, and $kC_{\mathrm{Dr}}^{1/2}C_{\mathrm{Er}}^{-1}$ values.

In summary, in stable stratification especially, measurements of L and the forms chosen for ψ_{m} and ψ_{h} chosen are crucial to the results. But our quality controls eliminated cases of very stable stratification, where estimates of ψ_{m} and ψ_{h} diverge wildly. And we have already reviewed why we believe that Holtslag and De Bruin's (1988) ψ_{m} and ψ_{h} functions are best for treating stable stratification (Jordan et al., 1999; Andreas, 2002).

The tendency in Figure 1 is for z_0 to increase with increasing u_*. This behaviour is reasonable because it has long been argued that the roughness length of mobile surfaces subject to saltation, drifting, and blowing should increase as the square of u_* (e.g., Owen, 1964; Radok, 1968; Chamberlain, 1983). Still, at any given u_* in Figure 1, the z_0 values are quite scattered. Such scatter, however, is not uncommon in z_0 plots (e.g., Kitaigorodskii and Volkov, 1965; Joffre, 1982; Bintanja and Van den Broeke, 1995) because z_0 is essentially an exponential function of the measured quantities, u_* and U_{r} [see (12a)].

We can use (12a) to estimate the uncertainty in individual z_0 values and, thereby, to establish the basis for the scatter. Individual eddy-covariance measurements of the drag coefficient are typically presumed to be uncertain by ±20% (e.g., Foken and Wichura, 1996; Larsen et al., 2001). This uncertainty dominates the uncertainty in (12a) because ψ_{m} is a slowly varying function of r/L. Consequently, we can approximate the uncertainty in z_0 from

$$z_0 = r \exp\left\{ -\left[\frac{k}{C_{\mathrm{Dr}}^{1/2}(1 \pm 0.1)} + \psi_{\mathrm{m}}(r/L) \right] \right\}. \tag{13}$$

Using a binomial expansion and keeping only the first-order terms, we find that z_0 is uncertain by a factor of $\exp(\pm 0.1 kC_{\mathrm{Dr}}^{-1/2})$. Since z_0 is typically 1 mm, C_{Dr} is roughly 1.9×10^{-3}. Hence, to first order, the true z_0 value can range between 0.4 and 2.5 times the measured value. The scatter in Figure 1, therefore, does not surprise us.

To mitigate the effects of this scatter, we must invoke the law of large numbers. In other words, we try to collect enough data to reduce the error in the sample mean to zero. Then, if the measurement errors are randomly distributed, the sample mean should approach the true mean. In practice, we simply bin average the z_0 data.

Figure 2 therefore shows the 740 z_0 values from Figure 1 averaged in bins that are $0.02\,\mathrm{m\,s^{-1}}$ wide for the lower u_* values and 0.05–$0.1\,\mathrm{m\,s^{-1}}$ wide for the higher u_* values, where we have fewer data. Except for the two highest u_* bins, where we have only eight and one z_0 value, all bins contain at least 20

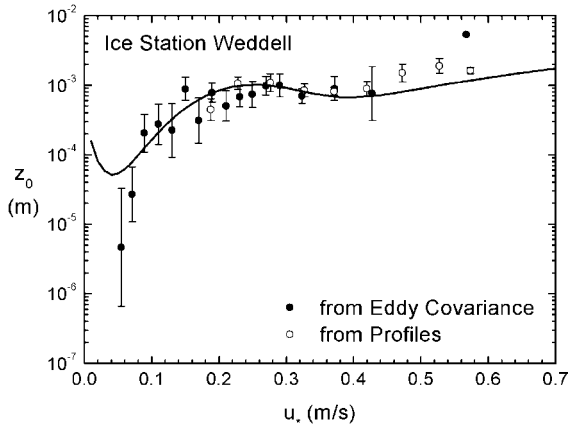

Figure 2. The z_0 values obtained from eddy-covariance and shown in Figure 1 are averaged in u_* bins. The plot also shows bin averages of 197 z_0 values that Andreas and Claffey (1995) deduced from a profile analysis. The error bars show ± 2 standard deviations in the mean z_0 value. The curve is Equation (19) with $F = 5$.

values and most have more than 40. To preserve the spread in the data that Figure 1 implies, our averaging in Figure 2 is logarithmic rather than arithmetic. That is, we summed the logarithms of the individual z_0 values rather than the values themselves to compute the averages displayed in Figure 2.

Andreas and Claffey (1995) had earlier estimated z_0 on ISW from 197 wind speed profiles collected in near-neutral stratification. Figure 2 also shows these profile-derived z_0 values, averaged in u_* bins typically $0.05\,\mathrm{m\,s^{-1}}$ wide.

That earlier analysis of z_0 values and drag coefficients (i.e., Andreas and Claffey, 1995; Andreas, 1995) convinced us that drifting and blowing snow is an important agent for setting the drag properties of snow-covered sea ice. Classical arguments based on converting the kinetic energy of particles in a saltation layer to potential energy (e.g., Owen, 1964; Radok, 1968; Chamberlain, 1983; Pomeroy and Gray, 1990) suggest that, above a threshold wind speed for drifting,

$$z_0 = \alpha \frac{u_*^2}{g}, \tag{14}$$

where α is a constant typically evaluated to be between 0.01 and 0.1.

In that earlier analysis, we identified $u_* = 0.30\,\mathrm{m\,s^{-1}}$ as the nominal threshold for drifting snow (cf. Bintanja, 2002). Below this threshold, the interplay between the wind and the macroscale roughness of the snow and ice sets the drag properties.

At still lower wind speeds, where the flow is aerodynamically smooth, molecular processes dictate the roughness length (e.g., Tennekes and Lumley,

1972, p. 156ff.). Laboratory data in neutrally stratified flow confirm that the flow speed profile in aerodynamically smooth flow obeys

$$\frac{U(z)}{u_*} = \frac{1}{k}\ln\left(\frac{u_* z}{\nu}\right) + B. \tag{15}$$

Here, z is the height above the surface, $U(z)$ is the flow speed at z, ν is the kinematic viscosity of the fluid, and B is a constant.

Equations (11), however, reflect the standard form of the wind speed profile in the atmospheric surface layer, which in neutral stratification is

$$\frac{U(z)}{u_*} = \frac{1}{k}\ln\left(\frac{z}{z_0}\right). \tag{16}$$

On comparing (15) and (16), we see that, in aerodynamically smooth flow, the roughness length must be (e.g., Monin and Yaglom, 1971, p. 287)

$$z_0 = \exp(-kB)(\nu/u_*). \tag{17}$$

With traditional values of $k = 0.40$ and $B = 5.0$ (Tennekes and Lumley, 1972, p. 157),

$$z_0 = 0.135(\nu/u_*) \tag{18}$$

in aerodynamically smooth flow.

We therefore model the roughness lengths in Figure 2 as the sum of three processes,

$$z_0 = \underbrace{\frac{0.135\nu}{u_*}}_{\text{(I)}} + \underbrace{0.035\frac{u_*^2}{g}\left\{F\exp\left[-\left(\frac{u_* - 0.18}{0.10}\right)^2\right]}_{\text{(II)}} + \underbrace{1\right\}}_{\text{(III)}}, \tag{19}$$

where $F = 5$. This is like the approach that Zilitinkevich (1969; also Smith, 1988) first suggested for parameterizing the roughness length of the open ocean except he had no Term II and his Term III derived from Charnock's (1955) wave argument rather than from the energetics of saltation. Fairall et al. (1996) later based the COARE bulk flux algorithm on such a summation of roughness lengths.

Our z_0 parameterization, however, has an extra term in it – Term II – to account for the fundamental macroscale roughness of the ice and snow surface. The work of Banke et al. (1980), Guest and Davidson (1991), Andreas and Claffey (1995), and Andreas (1995) provides the rationale for this term. All demonstrated that metre-scale roughness elements play a crucial role in dictating the drag properties of snow-covered sea ice. We model this term as a Gaussian: it therefore becomes negligibly small both at small u_*, where the momentum transfer is strictly by viscosity, and at large u_*, where blowing and drifting snow dominates the momentum transfer. Jordan et al. (2001) used a formulation like (19) in our preliminary ISW simulations with SNTHERM.

In concept, our (19) is quite similar to Raupach's (1991) parameterization for z_0 in terrestrial saltation layers. His model also acknowledges that the fundamental or 'permanent' surface roughness still influences z_0 for some range of u_* values above the saltation threshold. In our parameterization, this fundamental roughness has maximum effect for $u_* = 0.18\,\mathrm{m\,s^{-1}}$ and has at least a 10% effect on z_0 for all u_* values between 0.03 and $0.33\,\mathrm{m\,s^{-1}}$.

The one region in Figure 2 where the data do not agree with (19) is for the two smallest u_* bins, where the flow is aerodynamically smooth or in transition. Although Term I in (19) derives exclusively from laboratory observations in well controlled conditions that the natural atmosphere rarely replicates, others have reported atmospheric data compatible with Term I. That is, in measurements over the ocean in light winds, Geernaert et al. (1988) and Bradley et al. (1991) both show that the neutral-stability drag coefficient increases as the wind speed decreases toward zero.

These low-wind observations over the ocean, especially those of Bradley et al. (1991) in the western tropical Pacific, were likely made in unstable stratification. On the other hand, our low-u_* data come predominantly from stable stratification. The atmospheric boundary layer exhibits an array of behaviours in very stable stratification (i.e., in low winds) that we do not understand very well. It can be only intermittently turbulent, gravity waves are often present, the boundary layer may be so thin that (11) are not strictly accurate, and ψ_m and ψ_h are not well known. Coincidentally, we see the same disparity between (19) and our measurements of z_0 in our data at low u_* from SHEBA, the experiment to study the Surface Heat Budget of the Arctic Ocean (Andreas et al., 2003, 2004). Evidently, we still have more work to do to understand momentum transfer over snow-covered sea ice in light winds.

Equation (19) seems to be a fairly general result for snow-covered sea ice. We report elsewhere similar analyses we have done using eddy-covariance data collected during SHEBA (e.g., Andreas et al., 2001, 2003; Persson et al., 2002). Andreas et al. (2004) also found (19) useful in modelling these SHEBA z_0 measurements, but the F coefficient in Term II was 1 rather than 5. We understand the need for tuning this coefficient to the data because, we presume, this term represents the local features of the sea ice; and others have already established that the macroscale features of the sea ice determine its aerodynamic roughness (e.g., Banke et al., 1980; Overland, 1985; Guest and Davidson, 1991). Raupach (1991) also retained a site-specific underlying roughness in his parameterization of the roughness length of saltating surfaces.

3.2. Scalar roughness

Figures 3 and 4 show plots of the roughness lengths for temperature (z_T) and humidity (z_Q) nondimensionalized with z_0. Such plots are common in this

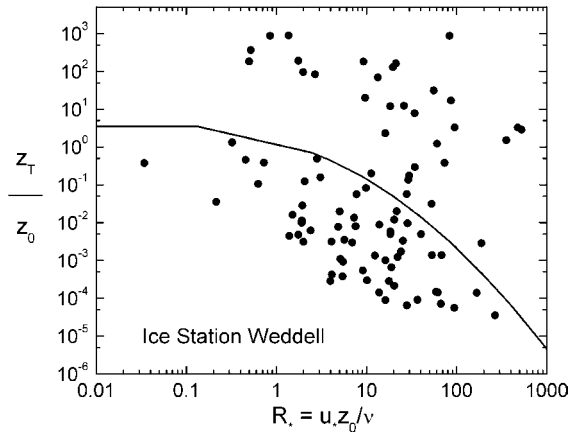

Figure 3. Ratios of temperature to momentum roughness (z_T/z_0) based on eddy-covariance measurements on Ice Station Weddell, where z_T comes from (12b). The horizontal axis is the roughness Reynolds number. The curve is Andreas's (1987) theoretical model, (22).

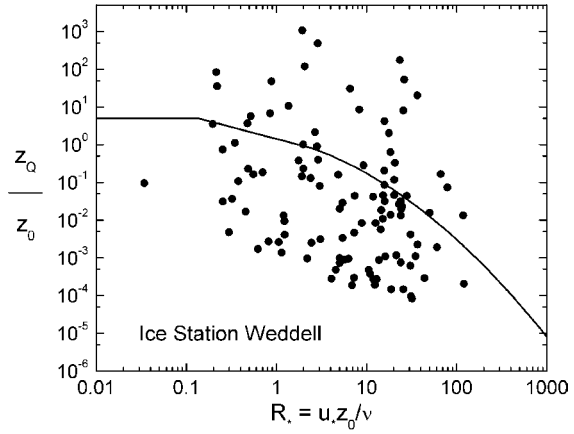

Figure 4. As in Figure 3 except these are ratios of humidity to momentum roughness (z_Q/z_0), where z_Q comes from (12c).

field (e.g., Garratt and Hicks, 1973; Munro, 1989; Bintanja and Van den Broeke, 1995) because, for neutral stability ($\psi_m = \psi_h = 0$), (11b) and (11c) can be written as

$$C_{sNr} = \frac{C_{DNr}}{1 - k^{-1} C_{DNr}^{1/2} \ln(z_s/z_0)}. \tag{20}$$

Here C_{DNr} is the neutral-stability drag coefficient at reference height r, C_{sNr} is the neutral-stability scalar transfer coefficient at r, and z_s is the scalar roughness – either z_T or z_Q. The advantage of (20) is that we need not

evaluate z_s and z_0 individually: The only quantities necessary to compute C_{sNr} are C_{DNr} and the ratio of the roughness lengths.

The z_T and z_Q data in Figures 3 and 4 had to pass our quality controls. We eliminated some data because of the constraints we placed on z_0, as discussed in the last sub-section, since knowing C_{Dr} is necessary for finding z_T and z_Q [see (12b), (12c), and (20)]. Further, to ensure good signal-to-noise ratio in our z_T calculations, we eliminated any hours for which $|T_s - \Theta_r| < 0.5\,°C$ or $|H_s| < 5.0\,W\,m^{-2}$. Likewise, for the z_Q analysis, we eliminated hours for which $|Q_s - Q_r| < 1.0 \times 10^{-4}\,kg\,kg^{-1}$ or $|H_L| < 1.0\,W\,m^{-2}$.

Despite these quality controls, the data in Figures 3 and 4 are quite scattered. From (12b) and (12c), we can explain this scatter by estimating the uncertainty in z_T and z_Q. As with C_{Dr}, typical uncertainties in eddy-covariance measurements of C_{Hr} and C_{Er} are $\pm 20\%$ (e.g., DeCosmo et al., 1996). Thus, as we did for z_0, we can estimate the uncertainty in z_T, for example, as

$$z_T = r \exp\left\{ -\left[\frac{k\, C_{Dr}^{1/2}(1 \pm 0.1)}{C_{Hr}(1 \pm 0.2)} + \psi_h(r/L) \right] \right\}. \tag{21}$$

With some first-order approximations, this suggests that z_T is uncertain by a factor of $\exp(\pm 0.3\, k\, C_{Dr}^{1/2}\, C_{Hr}^{-1})$. With $k = 0.40$ and $C_{Dr} \approx 1.9 \times 10^{-3}$, as before, and with a typical value for C_{Hr} of 1×10^{-3}, we see that an individual measurement of z_T can range from about 1/200 to 200 times the true value. Measurements of z_Q would have comparable uncertainty. As with z_0, we must therefore try to collect enough data for the true behaviour of z_T and z_Q to emerge in the averages.

In Figures 3 and 4, the solid curve is Andreas's (1987) theoretical model, which predicts

$$\ln(z_s/z_0) = b_0 + b_1(\ln R_*) + b_2(\ln R_*)^2, \tag{22}$$

where $R_* = u_* z_0/\nu$ is the roughness Reynolds number. Table I gives the polynomial coefficients in (22) when z_s is either z_T or z_Q.

On average, the data in both Figures 3 and 4 tend to corroborate Andreas's (1987) prediction. Both z_T/z_0 and z_Q/z_0 decrease with increasing R_*, and both ratios have magnitudes that agree approximately with the model's predictions. In particular, the z_Q/z_0 plot (Figure 4) is the first meaningful test of Andreas's (1987) model for humidity roughness. A few sporadic measurements of z_Q or C_E over snow and ice have appeared in the literature (e.g., Hicks and Martin, 1972; Thorpe et al., 1973; King and Anderson, 1994); but for his recent review, Andreas (2002) found no data sets accurate enough or extensive enough to test the z_Q predictions of (22).

Besides the scatter, Figures 3 and 4 also suffer from a statistical problem. In both figures, z_0 appears on both axes. The nondimensional values plotted

TABLE I

Values of the coefficients to use in (22) for estimating the scalar roughness lengths in three aerodynamic regimes.

	$R_* \leq 0.135$	$0.135 < R_* < 2.5$	$2.5 \leq R_* \leq 1000$
	Smooth	Transition	Rough
Temperature (z_T/z_0)			
b_0	1.250	0.149	0.317
b_1	0	−0.550	−0.565
b_2	0	0	−0.183
Humidity (z_Q/z_0)			
b_0	1.610	0.351	0.396
b_1	0	−0.628	−0.512
b_2	0	0	−0.180

therefore have built-in correlation. Andreas (2002) discusses this problem and demonstrates that the shared z_0 is capable of producing the decreasing trend in z_s/z_0 with increasing R_* seen in the data. To mitigate this problem, in Figures 5 and 6, we plot bin-averaged values of z_T and z_Q alone as functions of a bin-averaged u_*, as do Bintanja and Reijmer (2001). As with the z_0 plot, the bin-averaging of the z_T and z_Q values here is logarithmic rather than arithmetic. Also in Figures 5 and 6, we show semi-theoretical relations for z_T and z_Q based on (19) and (22). We refer to these as semi-theoretical because

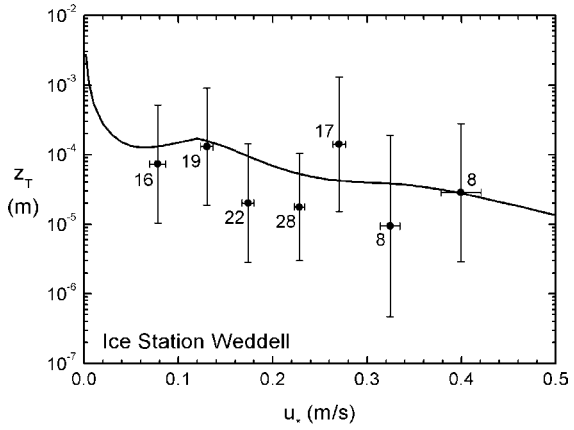

Figure 5. The z_T data depicted in Figure 3 are here averaged in u_* bins that are typically $0.05\,m\,s^{-1}$ wide. The error bars represent ± 2 standard deviations in the means of either z_T or u_*. The number beside each data marker gives the number of individual values in the bin. The curve derives from (19) and (22).

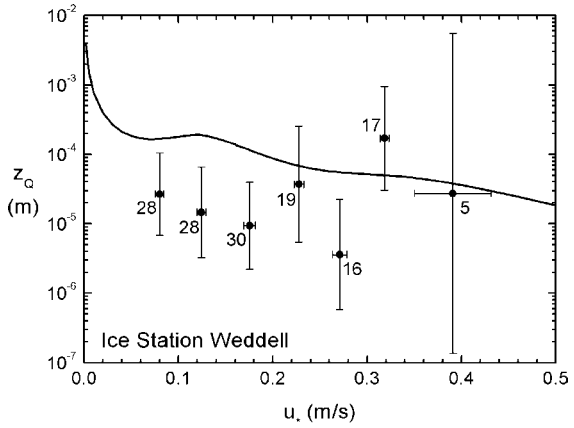

Figure 6. As in Figure 5 except this shows bin averages of the z_Q values depicted in Figure 4.

(22) derives from a theoretical model, while (19) has a theoretical basis but is tuned with ISW data.

The z_T data in Figure 5, in particular, seem to be well represented by the semi-theoretical model: All bin-averaged values are within two standard deviations of the model line. The z_Q data in Figure 6, on the other hand, are less compatible with the semi-empirical model, although the bin-averaged data are typically within an order of magnitude of the model. Our current understanding of interfacial scalar transfer provides no suggestion as to why Andreas's (1987) model should be appropriate for temperature but not for humidity. Therefore, we interpret Figure 6 as implying order-of-magnitude agreement between the ISW z_Q data and theory, but it also suggests enough disagreement to sound the call for more measurements of humidity transfer over snow and ice.

A reasonable interpretation of Figures 5 and 6 is that z_T and z_Q are essentially constants for u_* less than about $0.4\,\mathrm{m\,s^{-1}}$, with values of $4.1 \times 10^{-5}\,\mathrm{m}$ and $2.0 \times 10^{-5}\,\mathrm{m}$, respectively. These values are at odds with Bintanja and Reijmer's (2001) results, however. They conclude that, for $u_* \leq 0.30\,\mathrm{m\,s^{-1}}$, $z_T = z_Q = 2 \times 10^{-4}$, the nominal value that our semi-theoretical model predicts for $0.05 < u_* < 0.12\,\mathrm{m\,s^{-1}}$ (see Figures 5 and 6). Bintanja and Reijmer suggest that, when u_* values are above the drifting snow threshold of $0.30\,\mathrm{m\,s^{-1}}$, both z_T and z_Q increase as high powers of u_*. Although we have only a few dozen measurements of z_T and z_Q for u_* above $0.30\,\mathrm{m\,s^{-1}}$, we see no evidence of such an increase for large u_* in any of Figures 3–6.

4. Conclusions

We reported our analyses of over three months of eddy-covariance measurement over snow-covered sea ice on Ice Station Weddell. From these, we (i)

derived a new parameterization for the momentum roughness, z_0; (ii) verified a theoretical parameterization for the roughness length for temperature, z_T; and (iii) presented the largest data set yet reported that allows evaluating the roughness length for humidity, z_Q, over snow and ice.

Our analysis of z_0 suggests three regimes. Laboratory observations in aerodynamically smooth flow suggest that z_0 goes as ν/u_* in such conditions, but our data tend to be biased low in this regime. In high winds, nominally for u_* above $0.30\,\mathrm{m\,s^{-1}}$, saltation, blowing, and drifting occur, and z_0 goes as u_*^2/g. Between these two extremes is a region where z_0 plateaus. Here z_0 seems to depend on the macroscale or 'permanent' roughness of the surface. We model the contribution to z_0 here as a Gaussian function centered on a u_* value of $0.18\,\mathrm{m\,s^{-1}}$.

The z_T data tend to confirm Andreas's (1987) theoretical model for this quantity. Though our z_Q dataset is the most comprehensive yet available for snow or ice surfaces (cf. Andreas, 2002), it is less conclusive. Average z_Q values are typically within an order of magnitude of Andreas's (1987) model but tend to be below it for u_* values less than $0.30\,\mathrm{m\,s^{-1}}$. Because the latent heat flux over sea ice commonly has small magnitude and since z_Q is used to evaluate the latent heat transfer coefficient through a function that depends logarithmically on z_Q [i.e., (11c)], this discrepancy in not especially worrisome.

Neither the z_T nor the z_Q data support the assumption, common in large-scale models, that $z_T = z_Q = z_0$. Rather, our data tend to support Andreas's (1987) prediction that only in aerodynamically smooth flow are z_T and z_Q near z_0. As the flow gets aerodynamically rougher, the data show that z_0 increases over snow-covered surfaces, while z_T and z_Q tend to decrease.

Acknowledgements

We thank Boris V. Ivanov and Kerry J. Claffey for assisting with the data collection and processing and Emily B. Andreas for helping with the data processing. The National Science Foundation supported this research with awards OPP-98-14014 and OPP-00-84190, and the U.S. Department of the Army supported it through project 4A1611AT24.

References

Andreas, E. L: 1987, 'A Theory for the Scalar Roughness and the Scalar Transfer Coefficients over Snow and Sea Ice', *Boundary-Layer Meteorol.* **38**, 159–184.

Andreas, E. L: 1995, 'Air-Ice Drag Coefficients in the Western Weddell Sea: 2. A Model Based on Form Drag and Drifting Snow', *J. Geophys. Res.* **100**, 4833–4843.

Andreas, E. L: 2002, 'Parameterizing Scalar Transfer over Snow and Sea Ice: A Review', *J. Hydrometeorol.* **3**, 417–432.

Andreas, E. L and Cash, B. A.: 1996, 'A New Formulation for the Bowen Ratio over Saturated Surfaces', *J. Appl. Meteorol.* **35**, 1279–1289.

Andreas, E. L and Claffey, K. J.: 1995, 'Air-Ice Drag Coefficients in the Western Weddell Sea: 1. Values Deduced from Profile Measurements', *J. Geophys. Res.* **100**, 4821–4831.

Andreas, E. L and Treviño, G.: 1996, 'Detrending Turbulent Time Series with Wavelets', in G. Treviño, J. Hardin, B. Douglas, and E. Andreas (eds.), *Current Topics in Nonstationary Analysis*, World Scientific, Singapore, River Edge, NJ, pp. 35–73.

Andreas, E. L and Treviño, G.: 1997, 'Using Wavelets to Detect Trends', *J. Atmos. Oceanic Tech.* **14**, 554–564.

Andreas, E. L, Claffey, K. J., and Makshtas, A. P.: 2000, 'Low-Level Atmospheric Jets and Inversions over the Western Weddell Sea', *Boundary-Layer Meteorol.* **97**, 459–486.

Andreas, E. L, Fairall, C. W., Grachev, A. A., Guest, P. S., Horst, T. W., Jordan, R. E., and Persson, P. O. G.: 2003, 'Turbulent Transfer Coefficients and Roughness Lengths over Sea Ice: The SHEBA Results', in CD-ROM of preprints, *7th Conference on Polar Meteorology and Oceanography*, 12–16 May 2003, Hyannis, MA, American Meteorological Society, 9 pp.

Andreas, E. L, Fairall, C. W., Guest, P. S., and Persson, P. O. G.: 2001, 'The Air-Ice Drag Coefficient for a Year over Arctic Sea Ice', in Preprint Volume, *6th Conference on Polar Meteorology and Oceanography*, 14–18 May 2001, San Diego, CA, American Meteorological Society, pp. 300–303.

Andreas, E. L, Hill, R. J., Gosz, J. R., Moore, D. I., Otto, W. D., and Sarma, A. D.: 1998, 'Statistics of Surface-Layer Turbulence over Terrain with Meter-Scale Heterogeneity', *Boundary-Layer Meteorol.* **86**, 379–408.

Andreas, E. L, Jordan, R. E., Guest, P. S., Persson, P. O. G., Grachev, A. A., and Fairall, C. W.: 2004, 'Roughness Lengths over Snow', in CD-ROM of preprints, *18th Conference on Hydrology*, 11–15 January 2004, Seattle, WA, American Meteorological Society, 8 pp.

Andreas, E. L, Jordan, R. E., and Makshtas, A. P.: 2004, 'Simulations of Snow, Ice, and Near-Surface Atmospheric Processes on Ice Station Weddell', *J. Hydrometeorol.*, in press.

Baldocchi, D. D., Hicks, B. B., and Meyers, T. P.: 1988, 'Measuring Biosphere-Atmosphere Exchanges of Biologically Related Gases with Micrometeorological Methods', *Ecology* **69**, 1331–1340.

Banke, E. G., Smith, S. D., and Anderson, R. J.: 1980, 'Drag Coefficients at AIDJEX from Sonic Anemometer Measurements', in R. S. Pritchard (ed.), *Sea Ice Processes and Models*, University of Washington Press, Seattle, pp. 430–442.

Bintanja, R.: 2002, 'A New Power-Law Relation for the Vertical Distribution of Suspended Matter', *Boundary-Layer Meteorol.* **104**, 305–317.

Bintanja, R. and Reijmer, C. H.: 2001, 'A Simple Parameterization for Snowdrift Sublimation over Antarctic Snow Surfaces', *J. Geophys. Res.* **106**, 31739–31748.

Bintanja, R. and Van den Broeke, M. R.: 1995, 'Momentum and Scalar Transfer Coefficients over Aerodynamically Smooth Antarctic Surfaces', *Boundary-Layer Meteorol.* **74**, 89–111.

Bohren, C. F. and Albrecht, B. A.: 1998, *Atmospheric Thermodynamics*, Oxford University Press, New York, 402 pp.

Bradley, E. F., Coppin, P. A., and Godfrey, J. S.: 1991, 'Measurements of Sensible and Latent Heat Flux in the Western Equatorial Pacific Ocean', *J. Geophys. Res.* **96**, 3375–3389.

Buck, A. L.: 1976, 'The Variable-Path Lyman-Alpha Hygrometer and its Operating Characteristics', *Bull. Amer. Meteorol. Soc.* **57**, 1113–1118.

Buck, A. L.: 1977, 'Lyman-Alpha Radiation Source with High Spectral Purity', *Appl. Optics* **16**, 2634–2636.

Chamberlain, A. C.: 1983, 'Roughness Length of Sea, Sand, and Snow', *Boundary-Layer Meteorol.* **25**, 405–409.

Charnock, H.: 1955, 'Wind Stress on a Water Surface', *Quart. J. Roy. Meteorol. Soc.* **81**, 639.

DeCosmo, J., Katsaros, K. B., Smith, S. D., Anderson, R. J., Oost, W. A., Bumke, K., and Chadwick, H.: 1996, 'Air-Sea Exchange of Water Vapor and Sensible Heat: The Humidity Exchange over the Sea (HEXOS) Results', *J. Geophys. Res.* **101**, 12001–12016.

Dozier, J. and Warren, S. G.: 1982, 'Effect of Viewing Angle on the Infrared Brightness Temperature of Snow', *Water Resour. Res.* **18**, 1424–1434.

Fairall, C. W., Bradley, E. F., Rogers, D. P., Edson, J. B., and Young, G. S.: 1996, 'Bulk Parameterization of Air-Sea Fluxes for Tropical Ocean-Global Atmosphere Coupled-Ocean Atmosphere Response Experiment', *J. Geophys. Res.* **101**, 3747–3764.

Fairall, C. W., Hare, J. E., Edson, J. B., and McGillis, W.: 2000, 'Parameterization and Micrometeorological Measurement of Air-Sea Gas Transfer', *Boundary-Layer Meteorol.* **96**, 63–105.

Finnigan, J. J., Clement, R., Malhi, Y., Leuning, R., and Cleugh, H. A.: 2003, 'A Re-Evaluation of Long-Term Flux Measurement Techniques. Part I: Averaging and Coordinate Rotation', *Boundary-Layer Meteorol.* **107**, 1–48.

Foken, Th. and Wichura, B.: 1996, 'Tools for Quality Assessment of Surface-Based Flux Measurements', *Agric. For. Meteorol.* **78**, 83–105.

Fuehrer, P. L. and Friehe, C. A.: 2002, 'Flux Corrections Revisited', *Boundary-Layer Meteorol.* **102**, 415–457.

Garratt, J. R.: 1992, *The Atmospheric Boundary Layer*, Cambridge University Press, Cambridge, New York, 316 pp.

Garratt, J. R. and Hicks, B. B.: 1973, 'Momentum, Heat and Water Vapour Transfer to and from Natural and Artificial Surfaces', *Quart. J. Roy. Meteorol. Soc.* **99**, 680–687.

Geernaert, G. L., Davidson, K. L., Larsen, S. E., and Mikkelsen, T.: 1988, 'Wind Stress Measurements during the Tower Ocean Wave and Radar Dependence Experiment', *J. Geophys. Res.* **93**, 13913–13923.

Gordon, A. L. and Lukin, V. V.: 1992, 'Ice Station Weddell #1', *Antarct. J. U. S.* **27**(5), 97–99.

Guest, P. S. and Davidson, K. L.: 1991, 'The Aerodynamic Roughness of Different Types of Sea Ice', *J. Geophys. Res.* **96**, 4709–4721.

Hicks, B. B. and Martin, H. C.: 1972, 'Atmospheric Turbulent Fluxes over Snow', *Boundary-Layer Meteorol.* **2**, 496–502.

Holtslag, A. A. M. and De Bruin, H. A. R.: 1988, 'Applied Modeling of the Nighttime Surface Energy Balance over Land', *J. Appl. Meteorol.* **27**, 689–704.

ISW Group: 1993, 'Weddell Sea Exploration from Ice Station', *Eos, Trans. Amer. Geophys. Union* **74**, 121–126.

Joffre, S. M.: 1982, 'Momentum and Heat Transfers in the Surface Layer over a Frozen Sea', *Boundary-Layer Meteorol.* **24**, 211–229.

Jordan, R. E., Andreas, E. L, and Makshtas, A. P.: 1999, 'Heat Budget of Snow-Covered Sea Ice at North Pole 4', *J. Geophys. Res.* **104**, 7785–7806.

Jordan, R. E., Andreas, E. L, and Makshtas, A. P.: 2001, 'Modeling the Surface Energy Budget and the Temperature Structure of Snow and Brine-Snow at Ice Station Weddell', in Preprint Volume, *6th Conference on Polar Meteorology and Oceanography*, 14–18 May 2001, San Diego, CA, American Meteorological Society, pp. 129–132.

Kaimal, J. C. and Finnigan, J. J.: 1994, *Atmospheric Boundary Layer Flows: Their Structure and Measurement*, Oxford University Press, New York, 289 pp.

Kaimal, J. C. and Gaynor, J. E.: 1991, 'Another Look at Sonic Thermometry', *Boundary-Layer Meteorol.* **56**, 401–410.

Kaimal, J. C., Gaynor, J. E., Zimmerman, H. A., and Zimmerman, G. A.: 1990, 'Minimizing Flow Distortion Errors in a Sonic Anemometer', *Boundary-Layer Meteorol.* **53**, 103–115.
King, J. C. and Anderson, P. S.: 1994, 'Heat and Water Vapour Fluxes and Scalar Roughness Lengths over an Antarctic Ice Shelf', *Boundary-Layer Meteorol.* **69**, 101–121.
Kitaigorodskii, S. A. and Volkov, and Yu, A.: 1965, 'On the Roughness Parameter of the Sea Surface and the Calculation of Momentum Flux in the Near-Water Layer of the Atmosphere', *Izv. Acad. Sci. USSR, Atmos. Oceanic Phys.* **1**, 566–574.
Larsen, S. E., Edson, J. B., Fairall, C. W., and Mestayer, P. G.: 1993, 'Measurement of Temperature Spectra by a Sonic Anemometer', *J. Atmos. Oceanic Tech.* **10**, 345–354.
Larsen, S. E., Yelland, M., Taylor, P., Jones, I. S. F., Hasse, L., and Brown, R. A.: 2001, 'The Measurement of Surface Stress', in I. S. F. Jones and Y. Toba (eds.), *Wind Stress over the Ocean*, Cambridge University Press, Cambridge, New York, 155–180.
Launiainen, J. and Vihma, T.: 1990, 'Derivation of Turbulent Surface Fluxes – An Iterative Flux-Profile Method Allowing Arbitrary Observing Heights', *Environ. Software* **5**, 113–124.
Makshtas, A. P., Timachev, V. F., and Andreas, E. L: 1998, 'Structure of the Lower Atmospheric Layer over Ice Cover of the Weddell Sea', *Russian Meteorol. Hydrol.* **10**, 68–75.
Makshtas, A. P., Andreas, E. L, Svyashchennikov, P. N., and Timachev, V. F.: 1999, 'Accounting for Clouds in Sea Ice Models', *Atmos. Res.* **52**, 77–113.
McMillen, R. T.: 1988, 'An Eddy Correlation Technique with Extended Applicability to Non-Simple Terrain', *Boundary-Layer Meteorol.* **43**, 231–245.
Monin, A. S. and Yaglom, A. M.: 1971, *Statistical Fluid Mechanics: Mechanics of Turbulence*, Vol. 1, MIT Press, Cambridge, MA, 769 pp.
Munro, D. S.: 1989, 'Surface Roughness and Bulk Heat Transfer on a Glacier: Comparison with Eddy Correlation', *J. Glaciol.* **35**, 343–348.
Overland, J. E.: 1985, 'Atmospheric Boundary Layer Structure and Drag Coefficients over Sea Ice', *J. Geophys. Res.* **90**, 9029–9049.
Owen, P. R.: 1964, 'Saltation of Uniform Grains in Air', *J. Fluid Mech.* **20**, 225–242.
Paulson, C. A.: 1970, 'The Mathematical Representation of Wind Speed and Temperature Profiles in the Unstable Atmospheric Surface Layer', *J. Appl. Meteorol.* **9**, 857–861.
Persson, P. O. G., Fairall, C. W., Andreas, E. L, Guest, P. S., and Perovich, D. K.: 2002, 'Measurements near the Atmospheric Surface Flux Group Tower at SHEBA: Near-Surface Conditions and Surface Energy Budget', *J. Geophys. Res.* **107** (C10), DOI 10.1029/2000JC000705.
Pomeroy, J. W. and Gray, D. M.: 1990, 'Saltation of Snow', *Water Resour. Res.* **26**, 1583–1594.
Radok, U.: 1968, *Deposition and Erosion of Snow by the Wind*, Research Report 230, U.S. Army Cold Regions Research and Engineering Laboratory, Hanover, NH, 23 pp.
Raupach, M. R.: 1991, 'Saltation Layers, Vegetation Canopies and Roughness Lengths', *Acta Mech.* (Suppl.) **1**, 83–96.
Schotanus, P., Nieuwstadt, F. T. M., and De Bruin, H. A. R.: 1983, 'Temperature Measurements with a Sonic Anemometer and its Application to Heat and Moisture Fluxes', *Boundary-Layer Meteorol.* **26**, 81–93.
Smith, S. D.: 1988, 'Coefficients for Sea Surface Wind Stress, Heat Flux, and Wind Profiles as a Function of Wind Speed and Temperature', *J. Geophys. Res.* **93**, 15467–15472.
Tennekes, H. and Lumley, J. L.: 1972, *A First Course in Turbulence*, MIT Press, Cambridge, MA, 300 pp.
Thorpe, M. R., Banke, E. G., and Smith, S. D.: 1973, 'Eddy Correlation Measurements of Evaporation and Sensible Heat Flux over Arctic Sea Ice', *J. Geophys. Res.* **78**, 3573–3584.
Warren, S. G.: 1982, 'Optical Properties of Snow', *Rev. Geophys. Space Phys.* **20**, 67–89.

Webb, E. K., Pearman, G. I., and Leuning, R.: 1980, 'Correction of Flux Measurements for Density Effects Due to Heat and Water Vapour', *Quart. J. Roy. Meteorol. Soc.* **106**, 85–100.

Zilitinkevich, S. S.: 1969, 'On the Computation of the Basic Parameters of the Interaction between the Atmosphere and the Ocean', *Tellus* **21**, 17–24.